ELSEVIER

Ultrasound in Med. & Biol., Vol. 22, No. 8, pp. 987–997, 1996

0301-5629/96 $15.00 + .00

PII: S0301-5629(96)00142-1

●*Original Contribution*

ULTRASONIC MEASUREMENT OF GLOMERULAR DIAMETERS IN NORMAL ADULT HUMANS

TIMOTHY J. HALL, MICHAEL F. INSANA, LINDA A. HARRISON and GLENDON G. COX
Department of Radiology, University of Kansas Medical Center, Kansas City, KS

(*Received* 29 *December* 1995; *in final form* 1 *July* 1996)

Abstract—The average size of acoustic scatterers and the integrated backscatter coefficient of kidney cortex were measured *in vivo* from 2–4 MHz for a group of 50 normal adult volunteers. Our goal was to determine the sensitivity of the ultrasonic measurements under clinical conditions by identifying biologic sources of estimation uncertainty. Based on 10 measurements on each kidney of each volunteer, the average glomerular diameter for the group was found to be 216 ± 27 μm (SD). Glomerular size was found to correlate with body surface area (r = 0.4), and the ratio of glomerular surface area to body surface area (GSA/BSA) was found to be constant throughout normal adult life with GSA/BSA = (8.24 ± 1.35) × 10^{-8} (SD). These results are consistent with histologic analyses found in the literature. Within an individual, 7% standard errors in GSA/BSA are typical. Biologic variability dominates the variance in scatterer size estimates in a group not matched for BSA, where it accounts for 47% of the variance. In a group of individuals matched for BSA, biologic variability accounts for only 21% of the variance; day-to-day variability accounts for 35% of the variance; and experimental parameters account for the remainder. If a deviation greater than 2 × SD is considered abnormal, then this technique can potentially detect changes in glomerular diameter as small as 30 μm within an individual. To detect abnormal GSA/BSA values for an individual, GSA/BSA would have to differ from the mean for that group by about 3.6 × 10^{-8} or about 40%. Therefore, at this time scatterer size estimates appear most reliable for tracking the progression of disease and treatment for an individual over time.

Key Words: **Ultrasound, Tissue characterization, Quantitative imaging, Kidneys, Glomerular size.**

INTRODUCTION

In 1992, over 206,000 Americans were treated for end-stage renal disease at a cost for therapy of $9.5 billion, and the incidence of this disease has increased by approximately 10% per year (The National Institutes of Health, 1995). Glomerular size is recognized as an important factor in the progression of glomerular disease and as a predictor of outcome in some renal disease types (Newbold et al. 1992). For example, glomerular hypertrophy appears to be a prerequisite for the development of glomerulosclerosis (Cortes et al. 1992). However, no diagnostic imaging modality can resolve an individual glomerulus *in vivo* to allow measurement of its dimensions. Glomeruli are far too small (approximately 200 μm in diameter in adults) to resolve with standard B-mode ultrasonography and provide too little contrast for visualization in x-ray imaging. The only method currently available is a histologic analysis of biopsy samples. Although biopsy results are the gold standard, there are risks to the patient and sampling problems, and the analysis is applied to nonperfused tissues.

Our work has focused on quantitative ultrasonic imaging of the renal cortex. By combining physically based analytical models for acoustic scattering in the kidney with measurements based on the echo signals from those tissues we obtain more detailed information than is available in standard B-mode images. For example, we can estimate the average size of scatterers, even in complex biologic media. Echo data from the renal cortex of dogs suggest that the dominant sources of backscattering in the 2–5-MHz frequency range are glomeruli. In the 5–10-MHz frequency range, the dominant sources of backscattering are small blood vessels, perhaps the arterioles that pass blood to and from the glomerulus (Insana et al. 1992; Insana et al. 1995). We found that, although the backscattered intensity is anisotropic, the scatterer size estimates are largely isotropic in both frequency ranges (Insana et al. 1991).

Address correspondence to: Timothy J. Hall, Department of Radiology, University of Kansas Medical Center, 3901 Rainbow Boulevard, Kansas City, KS 66160-7234, USA.

We have also shown that we can estimate scatterer sizes and integrated backscatter coefficients for regions small enough to produce images of these parameters (Insana et al. 1993; Insana and Hall 1990).

Our previous laboratory studies involved either *in vitro* or surgically exposed organs. In the present work we focus on estimating scatterer sizes (D) and integrated backscatter coefficients (IBC) under clinical conditions. Our results indicate that we can adequately compensate for the attenuation of the acoustic beam to allow *in vivo* measurements.

METHODS

This study involved 50 adult volunteers, primarily University of Kansas Medical Center employees and students. All volunteers reported no clinical history of renal or hepatic problems. A screening blood profile (Chemzyme Plus #7964, SmithKline Beecham, St. Louis, MO) was performed within 2 weeks of ultrasound data acquisition to indicate normal renal function. We obtained a roughly uniform distribution in subject age ranging from 18 to 65 years, with approximately equal numbers of males and females. Table 1 summarizes the relevant information for these volunteers. All volunteers gave informed consent prior to participation, consistent with Internal Review Board protocol.

Data acquisition

A commercially available ultrasonography system (Siemens Q2000) with a 3-MHz curved linear array (3C40) was used to acquire radio-frequency (RF) echo signals from both kidneys of each volunteer. The ultrasonography system was modified by the manufacturer to provide unprocessed analog RF echo signals and the timing signals necessary for synchronization. A custom digital gating system was used to select echo signals from within a region-of-interest. The digitized echo signals were stored off-line for later analysis. Figure 1 illustrates the experimental configuration. The −20-dB frequency range for the digitized echo signals from a reference phantom (described below) was approximately 2 to 4 MHz.

Two transducer contact points were used per kidney. Five regions-of-interest (ROI) were recorded at each contact point for a total of 10 ROIs per kidney. Each ROI contained 40 consecutive A-lines within the renal cortex. Independent ROIs were obtained by angling the transducer on the skin surface between breaths. We attempted to position the transducer such that A-lines were parallel to the long axis of the nephron structure to minimize the anisotropic effects on attenuation and backscattered intensity (Insana et al. 1991).

A 7-MHz transducer was used to measure overlying skin, fat and muscle layer thicknesses for each ROI. These measurements were used to compensate for acoustic attenuation losses in these layers as described in what follows. Muscle layer thicknesses were also measured on two volunteers using x-ray CT for comparison. Results were within 1 mm of the ultrasonography measurements, thereby validating the ultrasonography technique.

Data analysis

A modified version of the reference phantom method (Yao et al. 1990) for data analysis was used to estimate acoustic backscatter coefficients. With this method, a reference medium of known acoustic properties is scanned under the same experimental conditions as those used for tissue measurement. Backscatter coefficients in the tissue are proportional to the ratio of the power spectral densities in the tissue and reference medium and can be obtained as follows:

$$\sigma_t(k) = \frac{\overline{|S_t(k)|^2}}{\overline{|S_r(k)|^2}} \sigma_r(k) \exp\left[4R(\alpha_t(k) - \alpha_r(k))\right] \quad (1)$$

In this equation, σ is the backscatter coefficient, S is the power spectral density and α is the attenuation coefficient in the tissue t and reference medium r at spatial frequency $k = 2\pi f/c$ (f is temporal frequency and c is the sound speed in the medium). R is the distance from the transducer face to the center of the range-gated region. The bar over the squared magnitude of S indicates the mean value, which is obtained by calculating S for each A-line and averaging over A-lines. Scatterer sizes (D) were estimated from changes in the backscatter coefficient with frequency, as previously described (Insana and Hall 1990). Integrated backscatter coefficients (IBC) were estimated by averaging σ_t over the 2- to 4-MHz-analysis bandwidth.

To determine the number of uncorrelated A-lines in a ROI, the correlation coefficient was measured among adjacent A-lines from the reference phantom using (Trahey et al. 1986):

$$\rho = \frac{\sum_{i=1}^{m} (X_i - \bar{X})(Y_i - \bar{Y})}{\sqrt{\sum_{i=1}^{m} (X_i - \bar{X})^2 \sum_{i=1}^{m} (Y_i - \bar{Y})^2}} \quad (2)$$

where X_i and Y_i are the RF echo amplitudes of A-lines X and Y, respectively, at position i in the subregion of the echo data, and $\bar{X}$ and $\bar{Y}$ are the sample mean values. The correlation coefficient for every fourth A-line was

Table 1. Some relevant parameters of the 50 normal volunteers including an identification number (ID), their age, gender, height (H), weight (W), body surface area (BSA), acoustically estimated average glomerular diameter (D), integrated backscatter coefficient (IBC), glomerular surface area (GSA, from D estimates) and GSA/BSA.

ID	Age (years)	Gender	H (cm)	W (kg)	BSA (m^2)	D (μm)	IBC $\times 10^5$ (cm^{-1} sr^{-1})	GSA $\times 10^5$ (μm^2)	GSA/BSA ($\times 10^8$)
1	42	M	182.9	81.8	2.04	204.5	6.20	1.31	6.44
2	40	M	180.3	81.8	2.02	234.0	4.60	1.72	8.52
3	18	F	182.9	72.7	1.94	235.3	24.70	1.74	8.97
4	23	M	177.8	77.3	1.95	215.3	15.20	1.46	7.47
5	42	F	165.1	52.7	1.57	209.3	7.30	1.38	8.76
6	39	F	172.7	56.8	1.68	193.3	19.30	1.17	7.00
7	24	F	162.6	51.8	1.54	234.0	3.70	1.72	11.16
8	27	F	170.2	63.6	1.74	209.5	8.50	1.38	7.93
9	33	F	157.5	56.8	1.57	248.0	3.20	1.93	12.33
10	38	M	193.0	90.9	2.22	242.3	3.40	1.84	8.31
11	32	F	170.2	56.8	1.66	227.3	9.20	1.62	9.79
12	34	F	167.6	53.6	1.60	183.8	7.20	1.06	6.63
13	26	M	182.9	90.9	2.13	233.8	7.30	1.72	8.05
14	32	F	167.6	51.4	1.57	195.5	8.80	1.20	7.64
15	23	M	182.9	81.8	2.04	214.8	4.00	1.45	7.11
16	31	F	167.6	55.5	1.62	233.8	4.50	1.72	10.58
17	46	F	170.2	72.7	1.84	206.0	20.80	1.33	7.24
18	46	M	188.0	90.9	2.18	237.8	3.30	1.78	8.16
19	37	M	185.4	86.4	2.11	214.8	2.50	1.45	6.88
20	23	F	160.0	51.4	1.52	223.5	20.90	1.57	10.33
21	23	M	180.3	78.6	1.98	212.0	4.70	1.41	7.11
22	42	F	172.7	65.9	1.78	197.3	8.90	1.22	6.85
23	37	F	154.9	49.1	1.46	214.0	3.20	1.44	9.89
24	30	F	167.6	59.1	1.67	218.5	6.00	1.50	9.00
25	38	M	180.3	90.9	2.11	239.3	2.50	1.80	8.52
26	58	M	172.7	63.6	1.76	209.5	4.10	1.38	7.84
27	41	F	160.0	54.5	1.56	187.5	18.20	1.10	7.09
28	45	F	160.0	62.7	1.65	198.3	21.40	1.23	7.47
29	18	F	170.2	50.0	1.57	185.8	6.80	1.08	6.91
30	22	F	167.6	68.2	1.77	208.0	6.00	1.36	7.67
31	18	M	188.0	72.7	1.98	205.5	6.70	1.33	6.71
32	18	M	172.7	79.5	1.93	203.3	5.30	1.30	6.71
33	47	M	188.0	93.2	2.20	210.5	7.00	1.39	6.33
34	64	F	152.4	63.6	1.61	202.3	3.80	1.29	8.00
35	36	F	167.6	56.8	1.64	210.8	10.50	1.40	8.51
36	32	M	182.9	86.4	2.09	215.0	8.20	1.45	6.96
37	20	F	160.0	50.0	1.50	227.0	11.30	1.62	10.78
38	29	M	172.7	84.1	1.98	237.3	3.90	1.77	8.94
39	29	F	167.6	70.9	1.80	235.0	13.00	1.73	9.63
40	42	F	160.0	45.5	1.44	205.8	11.10	1.33	9.23
41	61	F	157.5	56.8	1.57	189.5	13.50	1.13	7.20
42	37	M	172.7	81.8	1.96	229.5	5.20	1.65	8.46
43	50	F	167.6	68.2	1.77	196.5	8.00	1.21	6.85
44	30	M	172.7	70.5	1.84	220.0	3.60	1.52	8.28
45	60	F	162.6	72.7	1.78	217.0	12.30	1.48	8.31
46	37	F	165.1	52.3	1.56	220.8	5.70	1.53	9.78
47	31	F	167.6	52.3	1.58	207.3	18.00	1.35	8.53
48	30	M	193.0	102.3	2.33	232.5	1.90	1.70	7.28
49	39	M	180.3	90.9	2.11	238.5	3.00	1.79	8.47
50	26	F	157.5	59.1	1.59	218.3	8.30	1.50	9.39

less than 0.1 for all system setup conditions. Thus, with a 10% criterion for decorrelation, there were 14 uncorrelated A-lines per ROI. Parameter estimates and their variances were based on these 14 uncorrelated A-lines per view. We discarded two-thirds of the RF data to compute the variance in parameter estimates unambiguously.

Attenuation coefficient values applied to the individual layers of tissue were those found in the literature. Table 2 shows the attenuation coefficients for each layer and the primary references from which they were determined.

Reference phantom. A reference phantom was constructed for this study using well-known procedures (Madsen et al. 1978). Agar (3 g/100 mL) was combined with a water–alcohol solution (10% n-propanol by volume) and heated until a clear solution was obtained. The solution was cooled in an ice-water bath to 70°C and graphite flakes (50 g/L,

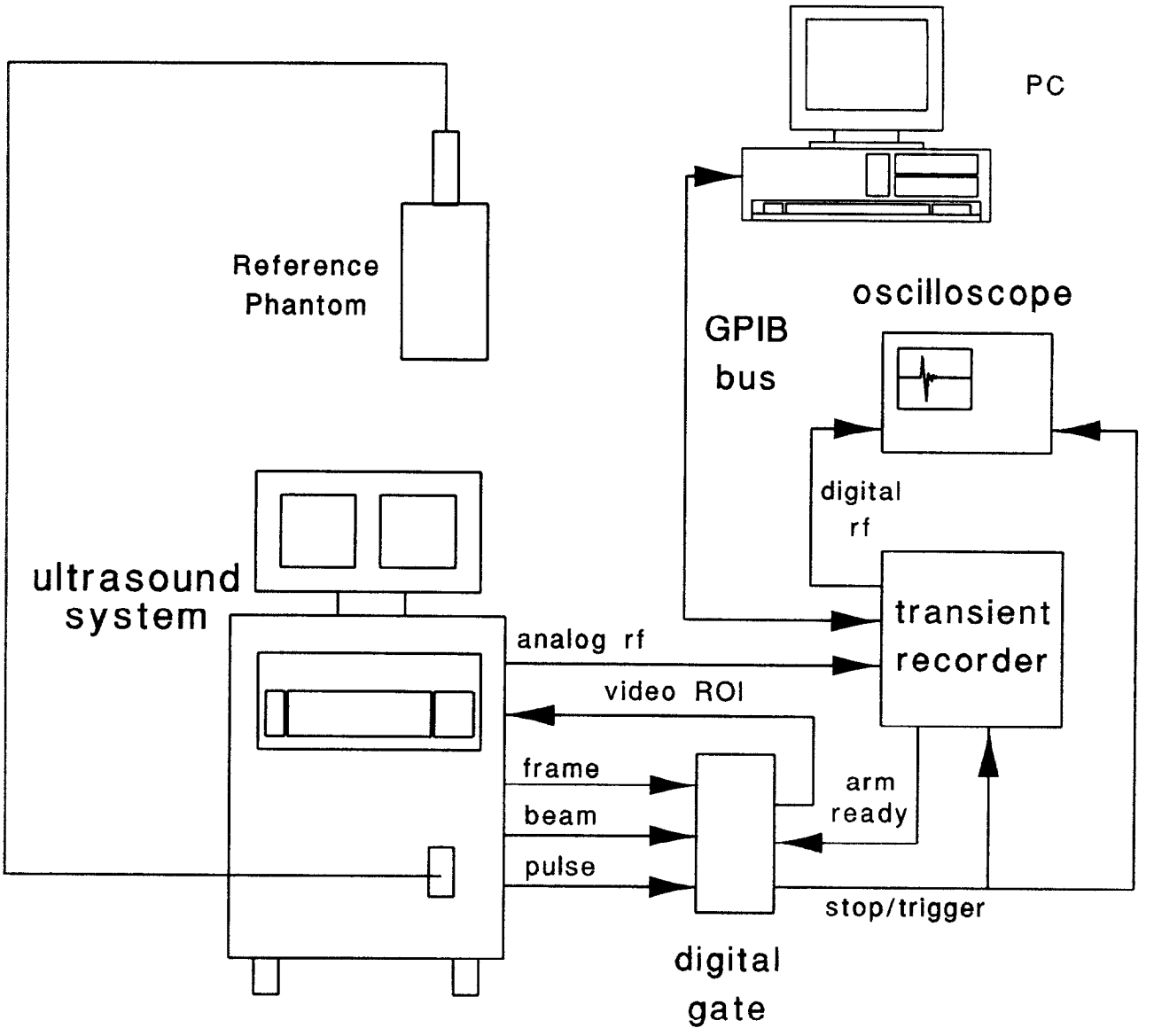

Fig. 1. An illustration of the experimental configuration used in data acquisition.

Fisher Scientific) were added. The solution was cooled to 40°C and poured into an acrylic plastic container. The container was rotated at 2 rpm until the mixture congealed. The container is a cylinder with acoustic windows on each end, which allowed acoustic properties to be measured using standard substitution techniques (Insana and Hall 1990; Madsen et al. 1982). The results are shown in Fig. 2.

Verification of data analysis in phantoms. The reference phantom technique for estimating backscatter coefficients and scatterer sizes was tested using three test samples with known scatterer sizes and number densities (samples 2, 4 and 8 of Insana et al. 1990). Echo waveforms were acquired using the Siemens Q2000, as described above, with the 3C40 curved linear array and 5-MHz and 7-MHz linear array transducers. The measured and pre-

Table 2. Attenuation parameters for each tissue layer involved in obtaining echo signals from *in vivo* kidney cortex.

Tissue	α_0	n	Reference
Skin	1.1	1.3	Reiderer-Henderson *et al.* (1988)
Fat	0.33	1.3	Goss *et al.* (1978, 1980)
Muscle	0.37	1.3	Goss *et al.* (1978), Daft and Briggs (1989)
Kidney	0.31	1.21	Insana *et al.* (1991)

Parameters correspond to attenuation coefficients fit to the model $\alpha(f) = \alpha_0 f^n$ where α is in dB/cm and f is in MHz.

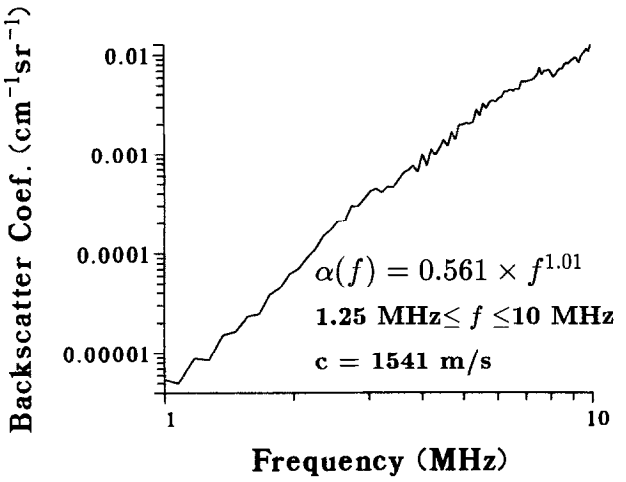

Fig. 2. A plot of the backscatter coefficient versus frequency for the reference phantom used in this study. In addition, the sound speed was 1541 m/s and the attenuation, in dB/cm measured at 11 frequencies from 1.25 to 10 MHz, was $\alpha(f) = 0.561 f^{1.01}$. Backscatter coefficients were measured from 1.25 to 3.5 MHz with a 2.25-MHz focused single element transducer with 100 RF A-lines from each of four different depths. Similar measurements were made with a 10-MHz transducer to obtain results from 2.5 to 10 MHz. These measurements were then averaged to obtain the plotted results.

dicted (Faran 1951) backscatter coefficients are plotted in Fig. 3. The corresponding scatterer size estimates are shown in Table 3.[1] Based on the data in Table 3 and Fig. 3, the reference phantom method is shown to provide accurate backscatter coefficient estimates, and therefore accurate D and IBC estimates, even when the reference medium and test samples have very different scattering properties.

RESULTS

Figures 4 and 5 show histograms of D and IBC estimates obtained from normal volunteers. Each estimate was computed from the average power spectrum for one ROI (14 uncorrelated A-lines). There are 980 estimates (some data were garbled in acquisition). The mean and standard deviation of each distribution are compared with other published data in Table 4.[2] Our lowest variance D estimates were obtained by averaging power spectra from the five ROIs per contact point, thus using 70 uncorrelated A-lines per estimate. Table 1 presents a summary of our results for each individual.

To evaluate measurement precision, we scanned volunteer number 35 nine times over a 5-day period. The skin was marked to aid in relocating the transducer from day-to-day. Measurements of overlying tissue layer thicknesses were also repeated. The results,

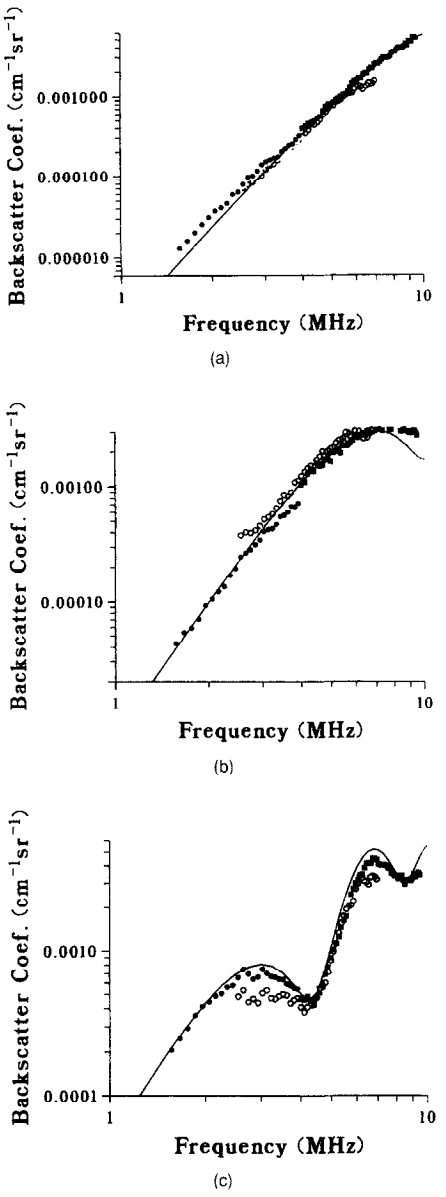

Fig. 3. Plots of the results of tests of the reference phantom method for estimating backscatter coefficients in three well-characterized phantoms. The solid line shows theoretical predictions; the solid circles, open circles and solid squares are for data acquired with the 3-, 5- and 7-MHz transducers, respectively. Parts (a), (b), and (c) show results for 41-μm, 75-μm, and 175-μm diameter glass bead phantoms, respectively.

[1] Scatterer sizes were estimated from echo signals from glass bead phantoms using Faran's (1951) scattering theory to obtain form factor models. These models allow scatterer size estimates in well-characterized media when the product of the wave number and scatterer radius $ka \geq 0.8$. Using the Gaussian form factor model, as is done in the renal cortex, scatterer size estimates are most accurate when $ka \approx 0.8$, as previously reported (Insana and Hall 1990).

[2] Ellis et al. (1989) and Nyengaard and Bendtsen (1992) reported volume estimates of the glomerular tuft. These data were converted to glomerular tuft diameters assuming a spherical model, and multiplied by a factor of 1.2 to estimate the diameter of Bowman's capsule, based on the reports of McLachlan et al. (1977) and Cohen (1975).

Table 3. Ultrasonically determined scatterer sizes D for the three glass bead phantoms used to test the reference phantom method for determining backscatter coefficients.

Transducer	Phantom					
Known dia.	41 ± 2 μm	*ka*	75 ± 3 μm	*ka*	175 ± 6 μm	*ka*
Measured dia.						
3C40	82 ± 20 μm	0.25	102 ± 7 μm	0.46	176 ± 4 μm	1.07
5L45	55 ± 8 μm	0.42	78 ± 6 μm	0.77	178 ± 2 μm	1.79
7L30	50 ± 5 μm	0.59	69 ± 4 μm	1.07	179 ± 6 μm	2.50

Glass bead diameters distributions were measured by the manufacturer and are NBS traceable, as described by Insana et al. (1990). The form factor model was based on the scattering model of Faran (1951). Note that D estimates are biased high for small *ka* (in the Rayleigh limit little information about the size or shape of the scatterer is conveyed). D estimates are accurate for $ka \approx 0.8$, and this accuracy can extend to large *ka* values if the form factor model is sufficiently accurate.

shown in Fig. 6, are plots of D and IBC estimates for left and right kidneys. The left kidney data, shown as solid circles, were obtained by scanning subcostally, whereas the right kidney data were obtained intercostally. The IBC estimates obtained intercostally show a much greater day-to-day variability in average values, relative to individual standard errors, and had a lower mean value, compared to those obtained subcostally. The D estimates were largely unaffected by intercostal versus subcostal data acquisition. We conjecture that inadvertent partial obstruction of the acoustic beam by a rib reduced the effective aperture of the transducer which would increase the scattering volume and reduce the magnitude and slightly alter the frequency content of the incident and scattered pressure fields. This would reduce backscatter coefficient estimates at all frequencies. Therefore, a partial obstruction of the beam should bias IBC estimates low and therefore increase the variance in IBC estimates, while having a lesser effect on the D estimates. Because of this finding, we focus our attention on D estimates throughout the remainder of this report. Combining data for kidneys of this individual we find a mean diameter of 211 μm and a variance of 372 μm^2.

Another potential source of variance in D estimates for a group of individuals is the age dependence in the size of renal microstructure, as reported by Darmady et al. (1973). Figure 7 shows estimates of glomerular diameter as a function of age measured acoustically and by microdissection techniques. Note that we have modeled glomeruli as spheres, and reduced the values reported by Darmady et al. (1973) by 25% for better comparison of the functional form in these two data sets. Our estimates were grouped into age ranges of 4 years to estimate a mean and standard error for each age group. The age dependence found in our data matches that of Darmady et al. (1973) fairly well. The bias among these two data sets is addressed in the "Discussion" section.

An alternative view of the changes in renal tissue as a function of age was described by Kasiske and

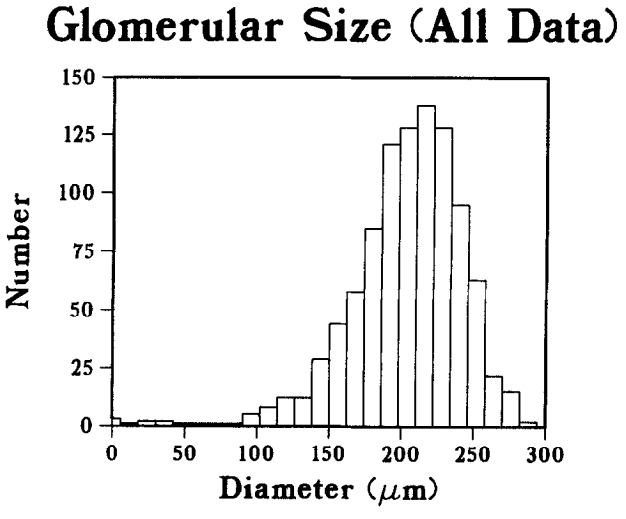

Fig. 4. A histogram of the glomerular size estimates for the group of 50 normal volunteers. Each estimate is based on the average power spectrum obtained from 14 uncorrelated A-lines in a given ROI (typically 10 estimates per kidney).

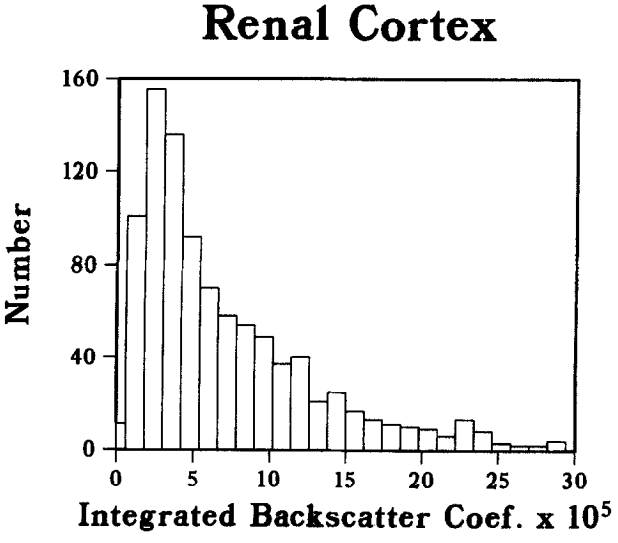

Fig. 5. A histogram of the integrated backscatter coefficient (sr^{-1} cm^{-1}) estimates for the group of 50 normal volunteers.

Table 4. Results of scatterer size (D) and integrated backscatter coefficient (IBC) estimates for N independent samples of normal human renal cortex.

Reference	N	D (μm)	IBC $\times 10^5$ (cm^{-1} sr^{-1})
Ultrasonic estimates			
Garra *et al.* (1994)	18	216 ± 35	7.4 ± 4
Wear *et al.* (1995)	11	232 ± 29	31 ± 15
	11	211 ± 57	23 ± 15
This study	50	216 ± 27	9.0 ± 9.8
Histologic estimates			
Darmady *et al.* (1973)	105	261	—
McLachlan *et al.* (1976)	32	164 ± 20	—
Dunnill and Halley (1973)	9	181	—
Ellis *et al.* (1989)	28	166	—
Newbold *et al.* (1992)	41	212	—
Nyengaard and Bendtsen (1992)	36	270	—

Ultrasonic estimates in each case were based on echo signals obtained from 2 to 4 MHz. Two sets of results were reported by Wear et al. (1993) corresponding to data obtained from two different imaging systems. See references for additional details regarding these studies.

Umen (1986) and later applied specifically to glomerular size by Nyengaard and Bendtsen (1992) and Newbold et al. (1992). Kasiske and Umen found that normal kidney weight was highly correlated with the body surface area (BSA) of the individual. BSA (m^2) was estimated using (DuBois and DuBois 1916) BSA = $0.007184 \times H^{0.725}W^{0.425}$, where H is the height (cm) and W is the weight (kg) of an individual. No correlation was found between kidney weight and age, gender or race once BSA was accounted for. The correlation between kidney weight and BSA was similar for normal and massively obese adults, and it was found that the increase in kidney weight among the obese group was proportional to increases in glomerular and tubule sizes (increased functional renal mass) (Kasiske and Umen 1986).

The functional capacity of the kidney varies with nephron size and number among humans (Dunnill and Halley 1973; McLachlan et al. 1977; Nyengaard and Bendsten 1992). As a newborn grows to adulthood, nephron size increases, but the number remains fixed until about the fourth decade of life. At that time, some glomeruli begin to sclerose, atrophy and eventually disappear (Darmady et al. 1973; Dunnill and Halley 1973; McLachlan et al. 1977; Nyengaard and Bendsten 1992). Thus, in the young, functional capacity is controlled by nephron size, and in the old, it may be controlled by both nephron size and number.

Glomeruli are approximately spherical in shape, and with that approximation we estimate the glomerular surface area GSA = πD^2. While the GSA and the BSA are correlated (Kasiske and Umen 1986; Newbold et al. 1992; Nyengaard and Bendsten 1992) the number of glomeruli and the BSA are not correlated (Nyengaard and Bendsten 1992). Therefore, the ratio GSA/BSA should be roughly constant within a given age group, and possibly throughout normal life. Figure 8 shows a plot of GSA/BSA as a function of age for our data and those from the histology literature (Nyengaard and Bendsten 1992) (tissues were formaldehyde-fixed and measured by fractionation sampling) and (Newbold et al. 1992) (tissues were formalin-fixed, paraffin-mounted and measured by manually digitizing the outline of Bowman's capsule), grouped

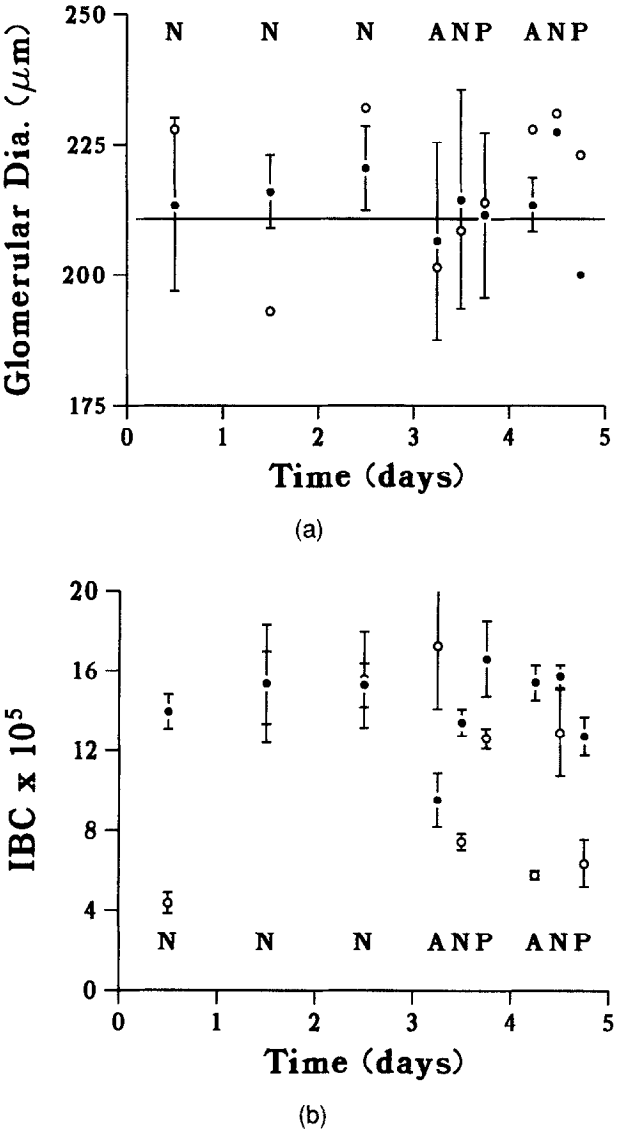

Fig. 6. Plots of the (a) glomerular size estimate and (b) integrated backscatter coefficient for one individual over a 5-day period. Measurements were made at noon on Monday, Tuesday and Wednesday, and at 7 am (A), noon (N) and 4:30 pm (P) on Thursday and Friday. Both left (solid circles) and right (open circles) kidney data are shown. Plotted values correspond to average power spectra from all five ROIs per contact point. Error bars correspond to 1 standard error among estimates for each ROI.

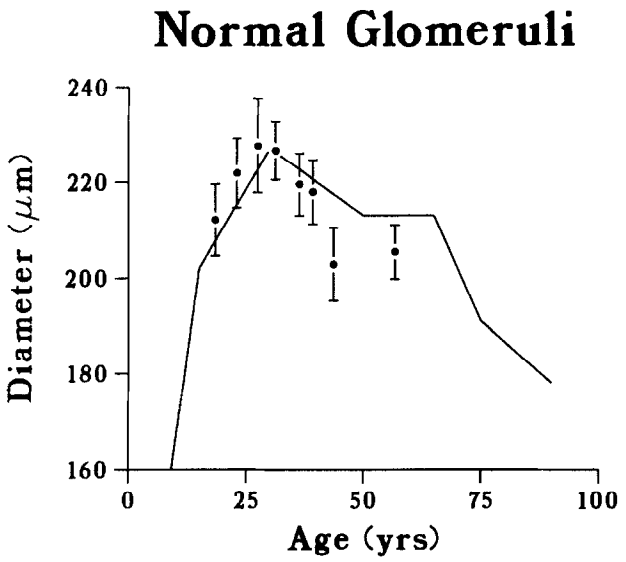

Fig. 7. A plot of the average glomerular size as a function of age. Data points are acoustically measured values for an age range of 4 years. The error bars represent one standard error for the group. The solid line shows the results published by Darmady et al. (1973), which have been reduced by 25% for comparison.

into 4-year age ranges. Normalizing the ultrasonically determined GSA estimates with BSA values eliminates the age-dependent variations in glomerular size.

Another source of estimation uncertainty is related to the size of the ROI. Assuming the acoustic scattering from glomeruli to be a stationary random process, the precision of echo signal power spectral density measurements should improve as the ROI is increased. However, kidneys are spatially heterogeneous and the acoustic attenuation in the cortex varies with the relative alignment between the acoustic beam and the nephron structure. Therefore, we carefully selected ROIs in which the acoustic beam was aligned with the nephron structure to determine the variance in scatterer size estimates, σ_D^2. We examined the dependence of σ_D^2 on the amount of data by selecting data from three females that were nearly identical in age, BSA and average D estimates (volunteers 7, 20 and 37), thus limiting other sources of biologic variability. The results, plotted in Fig. 9, indicate that the minimum variance achieved within one data set will be about 116 μm^2. This variability includes experimental uncertainties, such as scanning technique and regional and organ variability in the kidney microstructure.

An additional source of error in these estimates is caused by incomplete compensation of attenuation in the overlying tissues. The attenuation properties of skin, fat, abdominal muscle and kidney cortex are difficult to estimate in each individual because the layers are relatively thin. The values assumed in this work are different from those used in other studies (Garra et al. 1994; Wear et al. 1995). Reanalyzing data for a group of 14 volunteers using the attenuation values applied in those studies (i.e., 1.5, 0.46 and 0.51 dB/cm per MHz for skin, fat and muscle, respectively) increased the average D estimate from 224 μm to 251 μm, but had little effect on σ_D^2 (from 666 μm^2 to 634 μm^2). A more significant effect was found when the average values for layer thicknesses for overlying tissues were applied to all subjects instead of values measured for each individual. Applying these average values for attenuation correction resulted in a slight reduc-

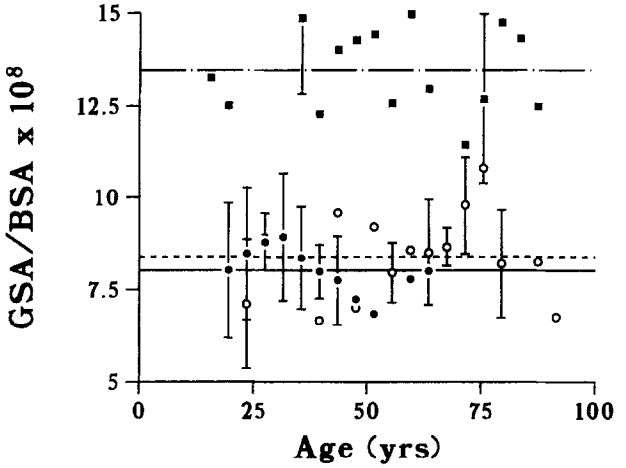

Fig. 8. A plot of the GSA/BSA ratio as a function of age. Included are data from this study and the average over all ages (solid circles, solid line), that of Newbold et al. (1992) (open circles, dashed line), and that of Nyengaard et al. (1992) (solid squares, dot-dash line). Error bars correspond to 1 standard deviation for that age group.

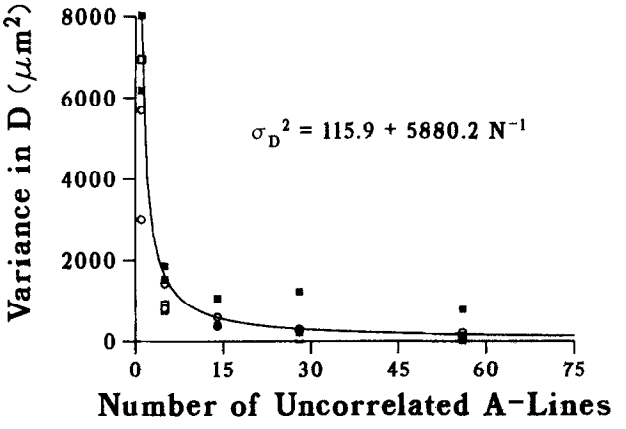

Fig. 9. A plot of the variance in glomerular diameter estimates as a function of the number of uncorrelated A-lines used to estimate the average power spectrum in the unknown medium (tissue). The data points correspond to values estimated for a group of individuals with roughly equivalent body size. (Note that there are two data points for each data symbol.) The solid line is the least squares fit of this data.

tion in the average D estimate from 224 μm to 213 μm and a significant increase in σ_D^2 from 666 μm^2 to 2069 μm^2. Therefore, to achieve the minimum variance in D estimates, it is very important to account for overlying tissue layer thicknesses for each individual.

By modeling the uncertainty in GSA/BSA estimates as the sum of independent sources of variance, we can determine the relative contribution of each source to the total variance of the population estimate. From a simple propagation of uncertainties:

$$\sigma^2_{GSA/BSA} = \frac{\sigma^2_{GSA}}{BSA^2} + \frac{\sigma^2_{BSA} \cdot GSA^2}{BSA^4} - 2r \cdot \frac{\sigma_{BSA} \cdot \sigma_{GSA} \cdot GSA}{BSA^3} \quad (3)$$

The correlation coefficient r between BSA and GSA in this study was 0.4 and is comparable to that found in histologic comparisons (Newbold et al. 1992; Nyengaard and Bendsten 1992). We assumed the DuBois (Dubois 1916) estimate of 1.3% for the average error in BSA; i.e., $\frac{\sigma_{BSA}}{BSA} \approx 0.013$. Then:

$$\sigma^2_{GSA/BSA} \approx \frac{\sigma^2_{GSA}}{BSA^2}\left(1 - 0.8\,\frac{\sigma_{BSA}/BSA}{\sigma_{GSA}/GSA}\right) \quad (4)$$

With the assumption that glomeruli are spherical, $\sigma_{GSA} = 2\pi D\sigma_D$. We identified three independent sources of variance in D estimates: ROI size, σ^2_{ROI}; day-to-day variations in the organ and measurement precision, σ^2_{d-d}; and biologic variability among individuals, σ^2_{biol}. That is:

$$\sigma^2_D = \sigma^2_{ROI} + \sigma^2_{d-d} + \sigma^2_{biol} \quad (5)$$

Our D estimates are based on averaging power spectra for 70 A-lines. Therefore, we can expect $\sigma^2_{ROI} \approx 200$ μm^2 (Fig. 9). The variance among nine repeat studies on the same person (Fig. 6) is modeled as $\sigma^2_D \approx \sigma^2_{ROI} + \sigma^2_{d-d}$. From those data, we estimate $\sigma^2_{d-d} \approx 372 - 200 = 172$ μm^2. Combining data for a group of seven individuals matched for gender, age and BSA (volunteers 9, 12, 14, 16, 35, 46 and 47), we obtained a total variance of 477 μm^2. This variance includes *ROI* variance and the day-to-day variance among this group (data were acquired at arbitrary times from 7 am to 7 pm). Therefore, among a gender-, age- and BSA-matched group, $\sigma^2_{biol,matched} \approx 477 - 372 = 105$ μm^2. The same approach can be used to obtain $\sigma^2_{biol,unmatched} \approx 715 - 372 = 343$ μm^2 among all 50 volunteers, 238 μm^2 above that for matched individuals. Table 5 summarizes the relative contribution to the total uncertainty in BSA/GSA estimates from each of these sources.

Pooling all 50 GSA/BSA estimates, our best estimate for GSA/BSA for normal adults is $(8.24 \pm 0.19; 1.35) \times 10^{-8}$ (standard error, standard deviation, respectively). Separating females from males, we found GSA/BSA = $(8.65 \pm 0.27; 1.49) \times 10^{-8}$ for females and GSA/BSA = $(7.63 \pm 0.18; 0.81) \times 10^{-8}$ for males which would appear to be a statistically significant difference. However, comparing females and males of similar BSA ($1.76 \leq BSA \leq 1.96$), we found no significant difference in GSA/BSA [GSA/BSA = $(7.93 \pm 0.41; 1.08) \times 10^{-8}$ for females, GSA/BSA = $(7.75 \pm 0.31; 0.70) \times 10^{-8}$ for males]. This suggests that BSA is not completely predictive of GSA in normal adults, as expected from the relatively low correlation coefficient. Results for an individual kidney indicate that GSA/BSA can be measured with about a 7% standard error.

DISCUSSION

The results reported here for the pooled group of volunteers are very similar to those reported by others using ultrasound (Garra et al. 1994; Wear et al. 1995), as shown in Table 4. Discrepancies among the means and variances of these reported results could easily be due to differences in the attenuation corrections used in overlying tissues and in the likely differences in the body sizes (BSA) of the study participants not accounted for in those studies.

The equivalence of GSA/BSA as a function of age suggests that this parameter could be more appropriate for comparing normal with diseased renal tissue. Excellent agreement was found between our estimates of GSA/BSA and that reported by others using independent techniques (Newbold et al. 1992). However, the large range of GSA/BSA values among a matched group of individuals suggests that further research is required before this is a clinically useful parameter for detecting an abnormal patient in a group of normals.

Significant disagreement still exists in the literature regarding the true size of glomeruli (Cortes et al. 1992), as shown in Table 4. The fixation and mounting processes used in preparing tissues for microscopy can shrink or swell soft tissues, like the renal cortex, depending on the processing (Elias and Hennig 1967). However, our measurements are in very good agreement with those in which formalin fixation was followed by paraffin mounting [a process found to have little effect on the kidney as a whole (Elias and Hennig 1967)]. Precision is of greater concern than accuracy when scatterer size estimates are used to detect changes over time. Consider, for example, the task of following the progression of disease and treatment where differ-

Table 5. The relative contribution to the total variance in parameter estimates from intrinsic sources (GSA/BSA estimate uncertainty is dominated by uncertainty in D estimates).

Source	Contribution to the estimate uncertainty in GSA/BSA		
	Variance (μm^2)	% of total (matched)	% of total (unmatched)
ROI	200	41	27
Day-to-day	172	35	23
Biol. (matched)	105	21	—
Biol. (unmatched)	343	—	47
BSA	—	3	3

ences in size may be important. The methods presented here are being developed to allow noninvasive serial measurement of glomerular diameter with negligible risk and relatively low cost.

One of the limits on the precision of our results is the spatial extent of the data used to estimate the average power spectrum in the tissue, as shown in Fig. 9. The thickness of the renal cortex limits the duration of individual A-lines. The curvature of the kidney limits the number of A-lines that are parallel to the nephron structure within each ROI. The large variability found for very small amounts of data (one A-line) suggests that simple periodogram techniques for spectral estimation will result in parametric images with high pixel variance (image noise). Parametric spectral estimates, such as autoregressive techniques, have shown some advantages in similar applications (Wear et al. 1993).

Accurate correction for frequency-dependent attenuation losses in overlying tissues is essential to obtain accurate estimates of glomerular sizes. The limited amount of data from these overlying layers results in poor *in vivo* attenuation estimates. Thus, assumptions based on published values were used. Fortunately, skin is very thin, and fat and muscle thicknesses overlying the kidney were typically only 1–3 cm thick in our group. Therefore, the penalty in parameter estimates due to small errors in attenuation correction was also relatively small.

CONCLUSIONS

In vivo glomerular size estimates, based on ultrasonic backscatter coefficient measurements, for normal volunteers are in excellent agreement with published values obtained histologically (when the swelling due to formalin fixing and the shrinking due to paraffin mounting in the histologic processing were accounted for). The ratio of ultrasonically determined glomerular surface area to body surface area was found to be roughly constant throughout normal adult life which suggests that the scatterer sizes measured acoustically at 2–4 MHz are indicative of glomerular diameters. Deviations from this range of values might eventually be used to indicate the presence of disease.

The variance in glomerular diameter estimates appears to be dominated by the contribution due to differences in body surface area. Among a group of individuals matched for age and BSA, the biologic variability was about half of that observed in the day-to-day variability in one individual. These variance estimates suggest that glomerular sizes can be estimated with approximately 10% precision.

The stability of glomerular size estimates within one person, and the fact that glomerular size is affected by a number of disease processes, suggests that this parameter may be very useful in tracking the progression of disease and treatment over time.

Acknowledgements—We are grateful for the support by NIH Grant No. R01 DK43007 and the Clinical Radiology Foundation, KUMC.

REFERENCES

Cohen AH. Massive obesity and the kidney. A morphologic and statistical study. Am J Pathol 1975;81:117–130.

Cortes P, Zhao X, Dumler F, Tilley BC, Atherton J. Age-related changes in glomerular volume and hydroxyproline content in rat and human. J Am Soc Nephrol 1992;2:1716–1725.

Daft CMW, Briggs GAD. The elastic microstructure of various tissues. J Acoust Soc Am 1989;85:416–422.

Darmady EM, Offer J, Woodhouse MA. The parameters of the aging kidney. J Pathol 1973;109:195–207.

DuBois D, DuBois EF. Clinical calorimetry. Arch Intern Med 1916;17:863–871.

Dunnill MS, Halley W. Some observations on the quantitative anatomy of the kidney. J Pathol 1973;110:113–121.

Elias H, Hennig A. Stereology of the human renal glomerulus. In: Weibel ER, Elias H, eds. Quantitative methods in morphology. New York: Springer-Verlag; 1967:130–166.

Ellis EN, Mauer SM, Sutherland DER, Steffs MW. Glomerular capillary morphology in normal humans. Lab Invest 1989;60:231–236.

Faran JJ. Sound scattering by solid cylinders and spheres. J Acoust Soc Am 1951;23:405–418.

Garra BS, Insana MF, Sesterhenn IA, Hall TJ, Wagner RF, Rotellar C, Winchester J, Zeman RK. Quantitative ultrasonic detection of parenchymal structural change in diffuse renal disease. Invest Radiol 1994;29:134–140.

Goss SA, Johnston RL, Dunn F. Comprehensive compilation of empirical ultrasonic properties of mammalian tissues. J Acoust Soc Am 1978;64:423–457.

Goss SA, Johnston RL, Dunn F. Comprehensive compilation of empirical ultrasonic properties of mammalian tissues II. J Acoust Soc Am 1980;68:93–108.

Insana MF, Hall TJ. Parametric ultrasound imaging from backscatter coefficient measurements: image formation and interpretation. Ultrason Imag 1990;12:245–267.

Insana MF, Wagner RF, Brown DG, Hall TJ. Describing small-scale structure in random media using pulse-echo ultrasound. J Acoust Soc Am 1990;87:179–192.

Insana MF, Hall TJ, Fishback JL. Identifying acoustic scattering sources in normal renal parenchyma from the anisotropy in acoustic properties. Ultrasound Med Biol 1991;17:613–626.

Insana MF, Wood JG, Hall TJ. Identifying acoustic scattering sources in normal renal parenchyma *in vivo* by varying arterial and ureteral pressures. Ultrasound Med Biol 1992;18:587–599.

Insana MF, Hall TJ, Wood JG, Yan Z-Y. Renal ultrasound using parametric imaging techniques to detect changes in microstructure and function. Invest Radiol 1993;28:720–725.

Insana MF, Wood JG, Hall TJ, Cox GG, Harrison LA. Effects of endothelin-1 on renal microvasculature measured using quantitative ultrasound. Ultrasound Med Biol 1995;21:1143–1151.

Kasiske BL, Umen AJ. The influence of age, sex, race, and body habitus on kidney weight in humans. Arch Pathol Lab Med 1986;110:55–60.

Madsen EL, Zagzebski JA, Banjavic RA, Jutila RE. Tissue mimicking materials for ultrasound phantoms. Med Phys 1978;5:391–394.

Madsen EL, Zagzebski JA, Frank GR. Oil-in-gelatin dispersions for use as ultrasonically tissue-mimicking materials. Ultrasound Med Biol 1982;8:227–287.

McLachlan MSF, Guthrie JC, Anderson CK, Fulker MJ. Vascular and glomerular changes in the aging kidney. J Pathol 1977; 121:65–78.

Newbold KM, Sandison A, Howie AJ. Comparison of size of juxtamedullary and outer cortical glomeruli in normal adult kidney. Virchows Arch A Pathol Anat 1992;420:127–129.

Nyengaard JR, Bendtsen TF. Glomerular number and size in relation to age, kidney weight, and body surface in normal man. Anat Rec 1992;232:194–201.

Riederer-Henderson MA, Olerud JE, O'Brien WD, Forster FK, Steiger DL, Ketterer DJ, Odland GF. Biochemical and acoustical parameters of normal canine skin. IEEE Trans Biomed Eng 1988;35:967–972.

The National Institutes of Health. Excerpts from the USRDS 1995 annual data report. Am J Kidney Dis 1995;26(4):Suppl 2.

Trahey GE, Smith SW, von Ramm OT. Speckle pattern correlation with lateral aperture translation: Experimental results and implications for spatial compounding. IEEE Trans Ultrason Ferroelec Freq Control 1986; UFFC-33:257–264.

Wear KA, Wagner RF, Insana MF, Hall TJ. Application of autoregressive spectral analysis to cepstral estimation of mean scatterer spacing. IEEE Trans Ultrason Ferroelec Freq Control 1993; UFFC-40:50–58.

Wear KA, Garra BS, Hall TJ. Measurements of ultrasonic backscatter coefficients in human liver and kidney in vivo. J Acoust Soc Am 1995;98:1852–1857.

Yao LX, Zagzebski JA, Madsen EL. Backscatter coefficient measurements using a reference phantom to extract depth-dependent instrumentation factors. Ultrason Imag 1990;12:58–70.